CHAPTER 4

SYNTHESIS AND CHARACTERIZATION OF $Ba(Ti_{1-x}Sn_xO_3)$ SYSTEM USING BARIUM NITRATE

4.1 INTRODUCTION

Barium titanate stannate, $Ba(Ti_{1-x}Sn_x)O_3$ is a binary solid solution system composed of ferroelectric barium titanate and non-ferroelectric barium stannate. This material system may find application for various purposes because the Curie temperature or dielectric constant of these types of system could be widely shifted by changing the wt% of tin in this scheme. The permittivity is very high as well as temperature is biased field sensitive. Therefore, it can be used in various potential applications, such as a capacitor, bolometer, actuator and microwave phase shifter [123].

The performance of BTS ceramics depends on the microstructure of sintered body, which is influenced by characteristics of the starting $Ba(Ti_{1-x}Sn_x)O_3$ powders. Synthesis of high-quality $Ba(Ti_{1-x}Sn_x)O_3$ nanopowders with better sinterability and improved dielectric properties is of great importance in advance research because of their large number of technological applications [124,125]. Therefore, attention has been focused on the synthesis of high-quality BTS nanopowders. Different chemical methods such as sol-gel [90], co-precipitation [92], low-temperature aqueous solution [91], low-temperature semi-wet [94] and combustion [95] have been used. These methods are not a cost-effective method for mass production of BTS powders for industrial applications. Thus preparation of $Ba(Ti_{1-x}Sn_x)O_3$ powders using solid state reaction method is regarded as one of the most practical and economical ways because it does not require

expensive chemicals as well as sophisticated equipment. This process is environment-friendly, and no toxic, or unwanted waste is produced after the solid state reaction is complete. This method is very much suitable for mass production of $Ba(Ti_{1-x}Sn_x)O_3$ powder for industrial applications. In the conventional solid-state reaction method powders of $Ba(Ti_{1-x}Sn_x)O_3$, powders are usually produced via the reaction between the mechanically mixed $BaCO_3$ or BaO, TiO_2 and SnO_2 particles at calcination temperature ≥1200 °C [126]. Unfortunately, the reactions are taking place such a high temperature, beyond control and the resultant powders often have a large particle size and wide size distribution, etc. It is reported in the literature that formation of $BaTiO_3$ and $BaSnO_3$ can take place at a lower temperature (600-700 ^{0}C) when $BaCO_3$ is replaced by $Ba(NO_3)_2$ [113].

4.2 RESULTS AND DISCUSSION

In the present discussion, polycrystalline samples of the system $BaTi_{1-x}Sn_xO_3$ where x=0.0, 0.1, 0.2 , 0.3 and 0.4 of this system are designated as BTS0, BTS10, BTS20 BTS30 and BTS40, respectively.

4.2.1 Thermal analysis of TiO_2 and $Ba(NO_3)$powder

The TG and DSC curves of TiO_2 and $Ba(NO_3)_2$ powders with a heating rate of 10^{o}C/min. in nitrogen atmosphere are shown in Figure 4.1 [(a), (b)] and Figure 4.2 [(a) , (b)] respectively. No weight change and peaks have been observed in the TG and DSC curves of TiO_2 powder in the temperature range 30 - 1000 ^{o}C. The TG curve of $Ba(NO_3)_2$ shows a single step weight loss (approximately 41%) in the temperature range 550^{o}C to 725 ^{o}C. The observed weight loss is in good agreement with the theoretical weight loss calculated according to be the reaction (4.1):

$$Ba(NO_3)_2 \rightarrow BaO + 2NO_2 + 1/2O_2 \qquad (4.1)$$

The DSC curve of $Ba(NO_3)_2$ shows two peaks at 587 ^oC and 708 ^oC. The first peak is attributed to melting of $Ba(NO_3)_2$ whereas second peak to the decomposition of $Ba(NO_3)_2$ to BaO according to the reaction (4.1). The observed melting temperature is approximately same as reported value 592 °C [127].

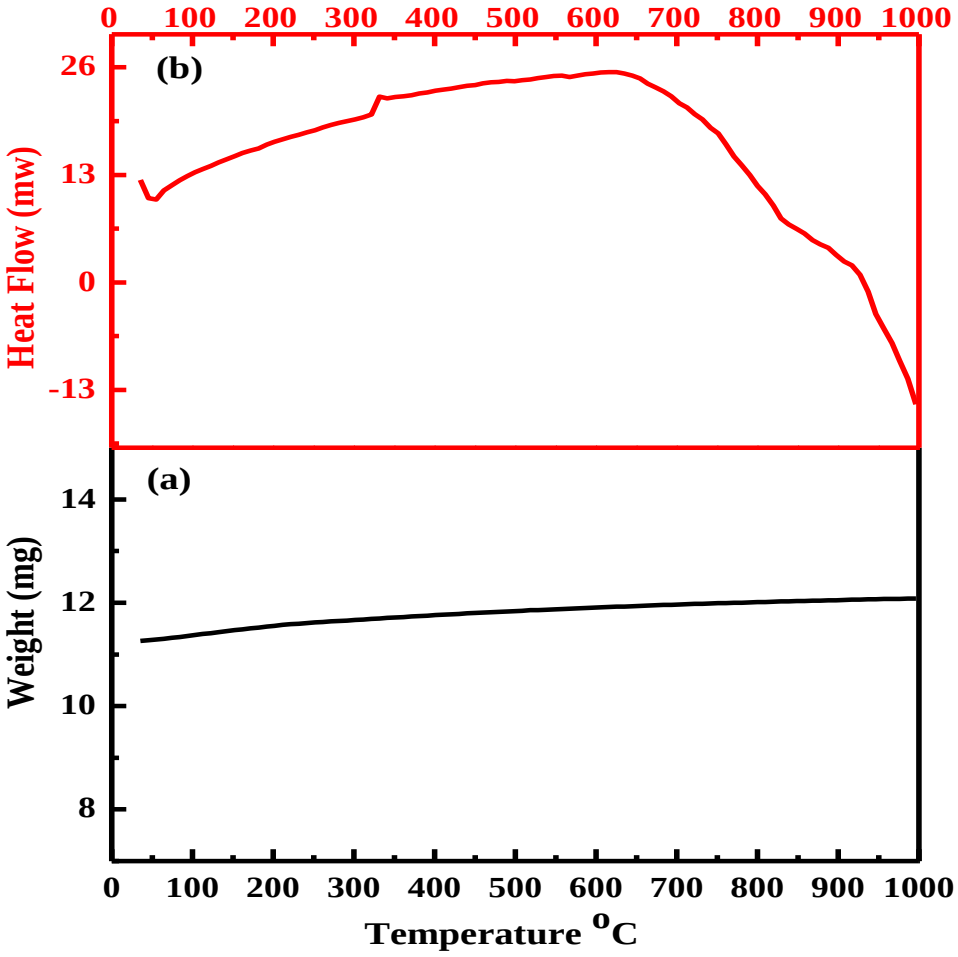

Figure 4.1 (a) TG and (b) DSC curve of TiO_2

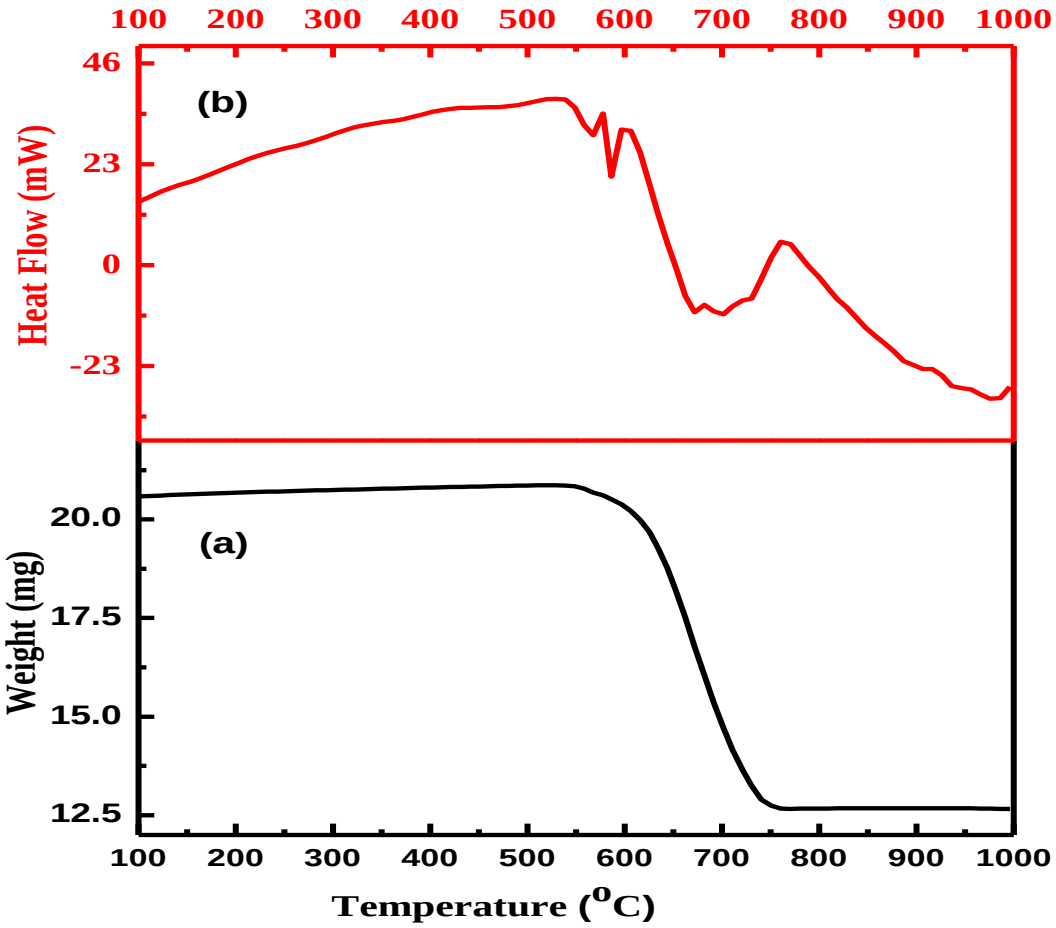

Figure 4.2 (a) TG and (b) DSC curve of $Ba(NO_3)_2$

4.2.2 Thermal Analysis of Mixture of Raw Materials for BTS20

For the synthesis of powders of BTS in this chapter raw materials $Ba(NO_3)_2$, TiO_2 and $SnCl_45H_2O$ have been used. Thermal analysis (TGA/DSC) of two raw materials $Ba(NO_3)_2$ and TiO_2 are already reported by us elsewhere [127]. Therefore, in this chapter, thermal analysis of third raw material $SnCl_45H_2O$ has been carried and shown in Figure 4.3 (a). TGA curve shows weight loss (90.46 %) in a single step between 50-250 ^oC, which is attributed to the decomposition of $SnCl_45H_2O$ to form SnO_2 according to reaction equation (4.2):

$$SnCl_4nH_2O \rightarrow SnO_2 + (n-2)H_2O + 4HCl \qquad (4.2)$$

In the DSC curve, two endothermic peaks at 60 ^oC and 150 ^oC have observed. The first peak is

attributed to evaporation of water and reaction product HCl whereas the second peak to decomposition of $SnCl_4$ according to reaction (4.2). The DSC curve of $SnCl_4\ 5H_2O$ used in this chapter is similar to DSC curve of this material reported in the literature [128].

TGA-DSC curves obtained for the stoichiometric mixture of $Ba(NO_3)_2$, TiO_2 and $SnCl_4 5H_2O$ for the sample BTS20 are displayed in Figure 4.2(b). The TGA curve shows total weight loss 40.24 % in two steps. The first step of weight loss (~ 10.05 %) in the temperature range 25-250 ^oC is attributed to the decomposition of $SnCl_4$ to form SnO_2 according to the reaction (4.2).

The second step of the weight loss (~30.19 %) in the temperature range 500-700 ^oC corresponds to the formation of solid solution $BaTi_{0.80}Sn_{0.20}O_3$ according to reaction

$$Ba(NO_3)_2 + 0.8TiO_2 + 0.2SnO_2 \rightarrow BaTi_{0.80}Sn_{0.20}O_3 + 2NO_2 + 0.5O_2 \qquad (4.3)$$

The weight loss of ~ 30.23 % observed experimentally is in agreement with the theoretical weight loss (30.19 %) calculated according to the reaction (4.3).

In the DSC curve, three endothermic peaks have been recorded. The first peak is attributed to the decomposition of $SnCl_4 5H_2O$, the second peak around 595 ^oC is assigned to the melting of $Ba(NO_3)_2$ and third peak at 630 ^oC to the reaction among molten $Ba(NO)_2$, solid TiO_2 and solid SnO_2 according to reactions (4.3) for the formation of desire solid solution $BaTi_{0.80}Sn_{0.20}O_3$. Based on these results it was decided to calcined mixtures of starting materials for all the compositions at 800^oC for 8h.

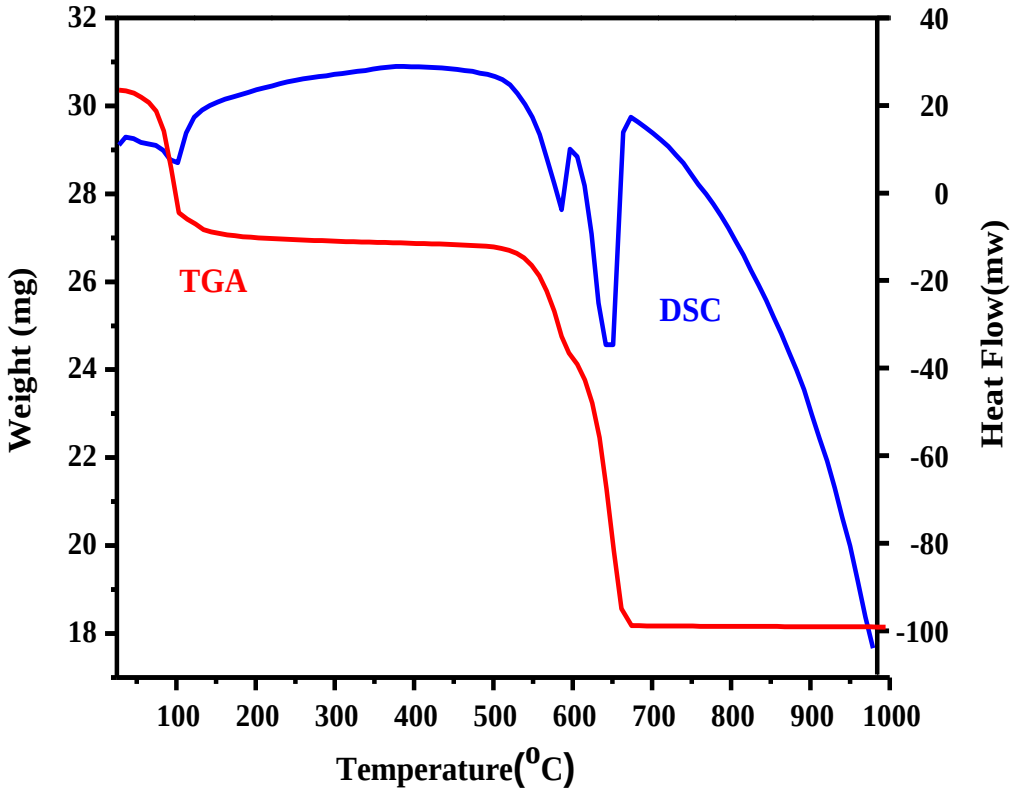

Figure 4.3 TGA-DSC curve of BTS20

4.3 CHARACTERIZATION OF CALCINED POWDERS

4.3.1 X-ray Diffraction (XRD)

Figure 4.4 (a) shows the room temperature XRD patterns of powders obtained after calcination at 800 ˚C for 8h. From this Figure, it is evident that except sample BTS40 all other samples are crystallized into single-phase solid solutions of the perovskite structure. To probe the crystal structure of synthesized powders the enlarged XRD patterns in the range of 2θ from 44 to 46° is shown in Figure 4.3 (b). Splitting of (200) and (002) peaks for samples BTS0 and BTS10 confirms tetragonal (JCPDS No. 05-0626) structure. Fusion of these peaks for the samples BTS20 and BTS30 indicates cubic structure (JCPDS No. 31- 0174). The incorporation

of Sn into the lattice of $BaTiO_3$ is also evident from the shifts of the peaks position toward lower values of 2θ angle side as the content of Sn increases. Structural parameters obtained from the XRD data of the samples are presented in Table 4.1. From the table, one can notice that lattice parameter increases with increasing Sn content. This refers to larger unit cell parameter induced by the partial replacement of Ti^{4+} (ionic radius 0.605 Å) by Sn^{4+} (ionic radius 0.69 Å) in octahedral sites.

The average crystallite size (D) of the calcined powders of all the samples has been calculated using Equation 2.2. These values are given in Table 4.1.

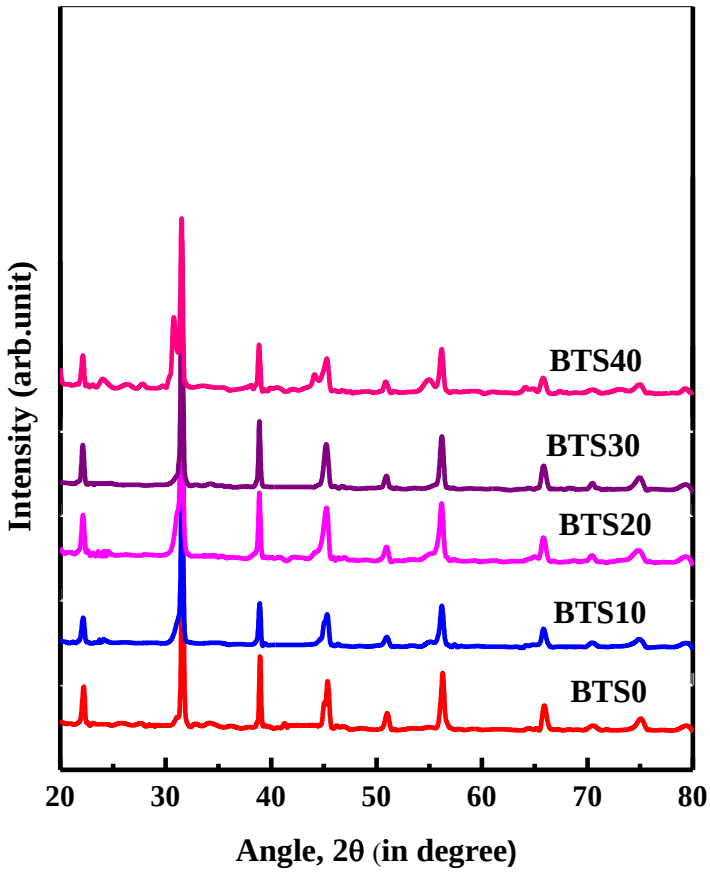

Figure 4.4 (a) XRD patterns of the calcined powders of the system $BaTi_{1-x}Sn_xO_3$

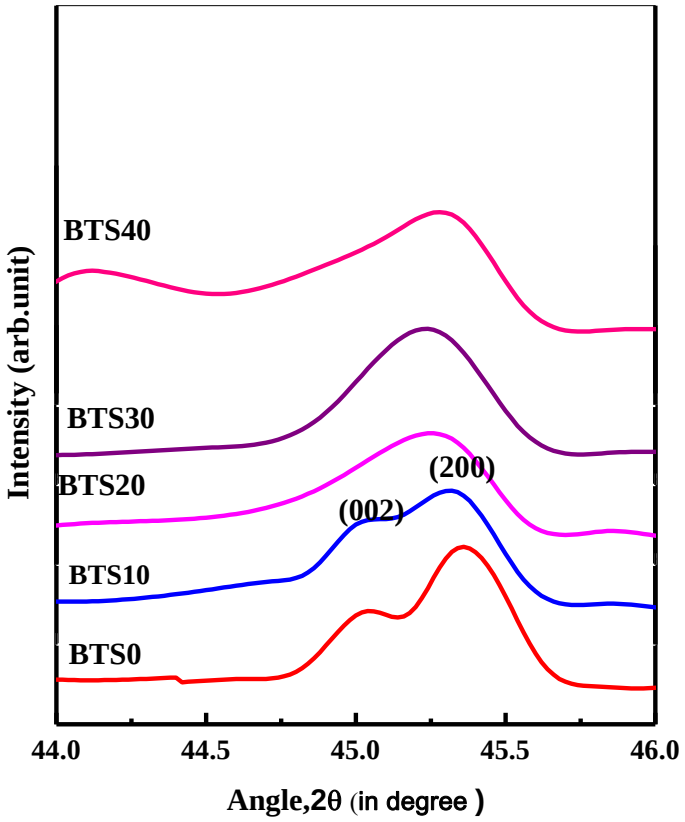

Figure 4.4 (b) Evolution of (002) and (200) peaks with increase in Sn concentration

Table 4.1 Structural parameters of $BaTi_{1-x}Sn_xO_3$ powders calcined at 800°C for 8h.

Composition (x)	Sample Code	Crystal Structure	Lattice parameter (Å)		Tetragonality (c/a)	Unit cell volume ($Å^3$)	Crystallite size (nm)
			a	c			
0.00	BTS0	T	3.9950(3)	4.0318(4)	1.0092	64.35	44
0.10	BTS10	T	4.0040(2)	4.0172(3)	1.0032	64.41	41
0.20	BTS20	C	4.0053(4)	------	1.0000	64.25	39
0.30	BTS30	C	4.0069(3)	------	1.0000	64.33	41
0.40	BTS40	Not a single phase	--------	-------	-----	--------	----

The earlier literature being told that the tetragonal structure of $BaTiO_3$ and single phase solid solutions of BTS ceramics can obtain at temperature ≥ 1200^oC when these samples are prepared by conventional solid state ceramic route using $BaCO_3$ and SnO_2 as starting materials [129]. Even if BTS powders are synthesized by chemical methods mentioned above, it is necessary to calcine the as-prepared powders at temperature ≥ 900^oC. The lower temperature of the formation of solid solution in this approach is due to the low melting temperature of starting materials $Ba(NO_3)_2$ and $SnCl_4.5H_2O$ used in this chapter. Raw material $Ba(NO_3)_2$ have a melting point of 592 °C [130] it has been verified by DSC analysis by us [127]. At reaction temperature (~ 630^oC) $Ba(NO_3)_2$ will take on a molten state which may increase the contact area with TiO_2 crystals and accelerate the response rate, leading to the lowered reaction temperature.

4.3.2 Transmission Electron Micrographs (TEM)

Figure 4.5 (a) and (b) show Transmission electron micrographs (TEM) of the calcined powder of sample BTS20 and histogram of the distribution of particle size obtained using software Image J software. The micrograph reveals that the powder particles are spherical in shape with an average particle size of 35±5 nm which is consistent with crystallite size ~39 nm (Table 4.1) calculated using Scherer's Equation (2.2).

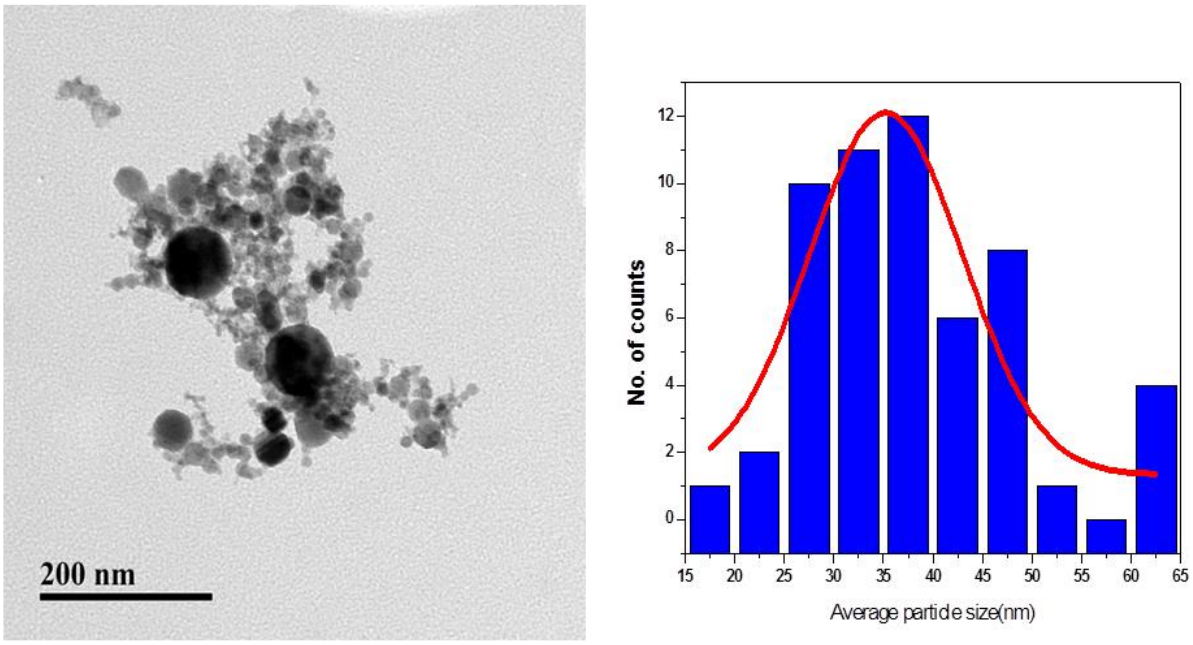

Figure 4.5 (a) Transmission Electron Micrograph of BTS20 (b) Gaussian Distribution plot for Particle size

4.4 CHARACTERIZATION OF CERAMICS

4.4.1 X-ray Diffraction (XRD)

Figure 4.6 shows the room temperature XRD patterns of BST ceramics sintered at 1350^{o}C for 4h. From the XRD patterns, it is evident that all the ceramic samples (x=0.0, 0.1, 0.2, 0.3 and 0.4) crystallized into single phase solid solutions of the perovskite structure. It is seen from the Figure 4.2(b) that the peaks are shifted to lower 2θ angles with the increasing of Sn concentration. This also indicates that $Sn^{4+}$is dissolved in the lattice of $BaTiO_3$ over a range of compositions we have studied. The absence of secondary phases suggests that the solubility of Sn is 40 % in $BaTiO_3$ lattice. The Rietveld refinement method of the X-ray diffraction patterns was used to obtain the lattice parameters of the ceramic samples and given in Table 4.2. The value of the lattice parameters increases with the increasing Sn content. The phase transition

from tetragonal to cubic structure and increase in the lattice parameters on increasing concentration of Sn in the lattice of $BaTiO_3$ are according to the literature [54]. On comparing the value of tetragonality reported in Table 4.1 with Table 4.2, it is found that tetragonality increases with increasing temperature. The bulk density (d_b) of the sample synthesized at 1000 ^oC was obtained using Archimedes' principle. Theoretical density (d_{th}) of the samples was calculated from the molecular weight of the samples and lattice parameters. The % porosity was calculated using the equation 2.3. The value of % porosity of all the samples is presented in Table 4.2.

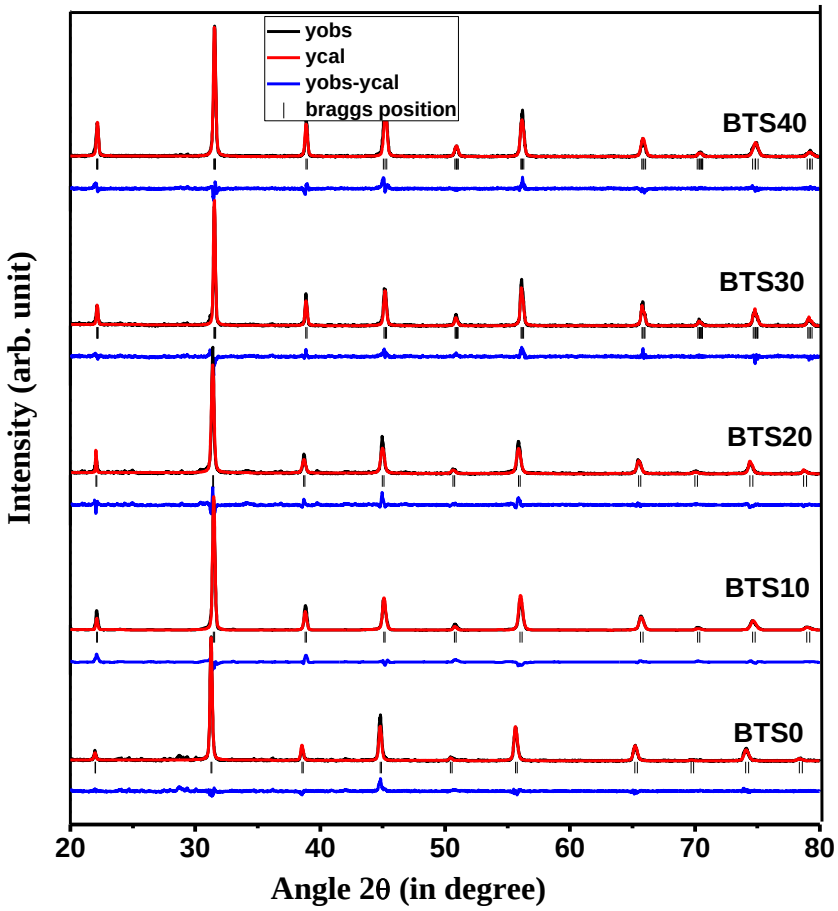

Figure 4.6 XRD pattern of the sintered sample of $BaTi_{1-x}Sn_xO_3$

Table 4.2 Structural parameters of $BaTi_{1-x}Sn_xO_3$ ceramics sintered at 1350 ^oC for 4h

Sample Code	Structure	Lattice parameter (Å)		Tetragonality (c/a)	Cell volume ($Å^3$)	% Porosity	Grain size(μm)
		a	c				
BTS0	Tetragonal	3.9900(5)	4.0323(3)	1.0106	64.19	4	3.5
BTS10	Tetragonal	4.0113(3)	4.0312(4)	1.0049	65.09	6	3.2
BTS20	Cubic	4.0254(4)	4.0254(2)	1.0000	65.23	9	3.0
BTS30	Cubic	4.0338(3)	4.0338(6)	1.0000	65.64	9	2.7
BTS40	Cubic	4.0453(2)	4.0453(4)	1.0000	66.18	10	2.5

From the Table 4.2, it is clear that % porosity increases with increasing Sn concentration. The lattice parameters, tetragonality and relative density of the samples obtained in this chapter were analyzed through a comparative study with those reported in the literature and presented in Table 4.3 [54,109-112,123]. Comparatively higher tetragonality and density achieved in this work are attributed to nano-size of calcined powders on account of lower temperature (800 ^oC).

Table 4.3 Comparison of structural parameters of $BaTi1_{-x}Sn_xO_3$ ceramics

Preparation method	Composition (x)	Structure	Calcination		Sintering					References
			Temperature (^oC)	Time (h)	Temperature (^oC)	Time (h)	Cell Volume	Tetragonality	Density/ % porosity	
Solid State Reaction	0.00 0.10 0.20 0.30 0.40		1100	3	1250 1380 1380 1420 1420	2			5.81 6.04 6.14 6.24 6.21	17
Solid State Reaction	0.00 0.10 0.20	T T C	1200 1200 1200	3	1400	4	64.00(8) 64.57(5) 65.49(2)	1.0403 1.00201	5 8 12	18
Solid State Reaction	0.00 0.10 0.20		1100	4	1350	4				19
Solid State Reaction	0.00 0.10		1100	2	1370	5		1.0775 1,0048		20
Solid State Reaction	0.00 0.10 0.20		1200	3	1300	4		1.0031 1.0017		21
Sol –gel	0.10 0.20	T C	1000		1350	2			5.9 5.43	22
Solid State Reaction	0.0 0.10 0.20 0.30 0.40	T T C C C	800	8	1350	4	64.19 65.09 65.23 65.64 66.18	1.0108 1.0030 1.0000 1.0000 1.0000	4 6 8 9 10	This work

4.4.2 Raman Spectroscopy

Raman spectroscopy can detect lower concentrations of impurity phases and is more sensitive to non-crystalline phases than XRD. The structural information from the Raman spectra refers to single TiO_6 octahedral, whereas the symmetry found by XRD is due to an ensemble of unit cells of more than 10 nm^3 [131].Thus to investigate the local structure, room temperature Raman spectra of sintered samples were recorded and shown in Figure 4.6. The Raman spectrum of samples BTS0 ($BaTiO_3$) and BTS10 indicates the typical spectral signature of the tetragonal (T) ferroelectric phase of $BaTiO_3$, namely the presence of an interference effect at 180cm^{-1}, the sharp "silent" mode at 305cm^{-1} and the mode at 715cm^{-1}. These spectra have well agreed with that of the tetragonal $BaTiO_3$ reported for single crystal and powder in the literature [132,133]. By increasing the Sn content damping of these modes occurs, leading to their complete disappearance for BTS20, BTS30 and BTS40 samples. Raman pattern of BTS20, BTS30, and BTS40 samples agree with that of the cubic phase of $BaTiO_3$. Thus both XRD and Raman spectroscopy support phase transition from tetragonal to cubic as the concentration of Sn increases for BTS ceramic.

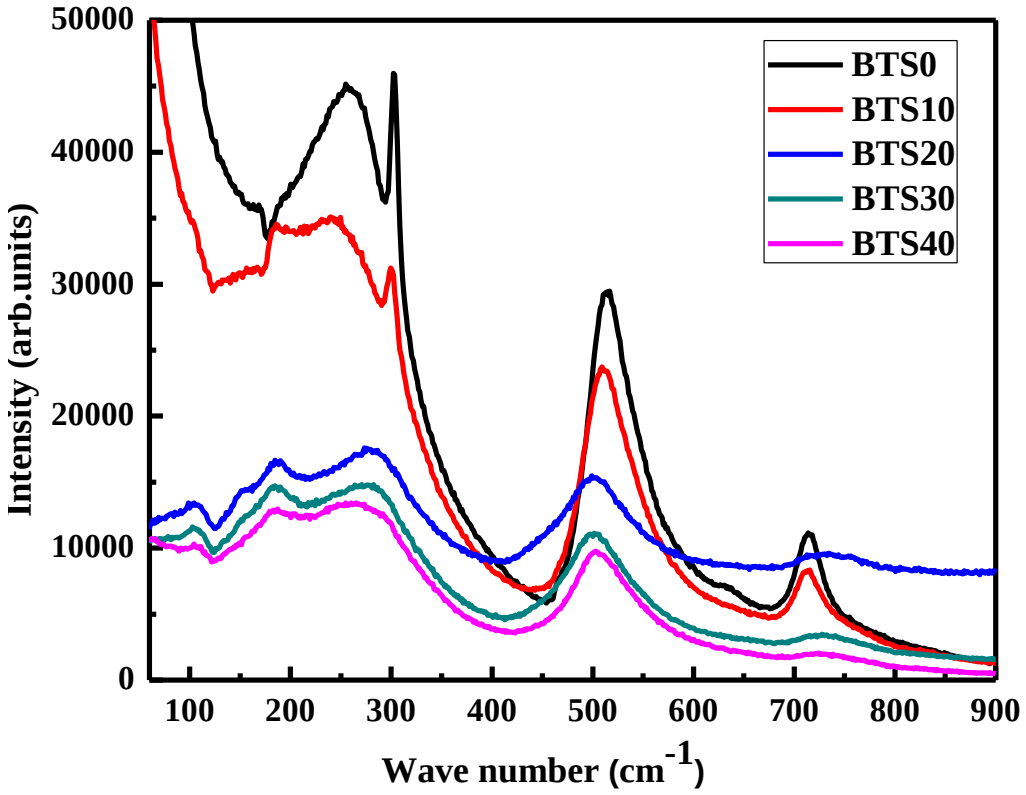

Figure 4.7 Room temperature Raman spectra of the sintered samples in the system $BaTi_{1-x}Sn_xO_3$

4.4.3 Fourier Transformed Infrared (FTIR) Spectroscopy

According to the reported literature, $BaCO_3$ is the most common impurity of the $BaTiO_3$ based powders prepared by any methods. FTIR was found to be the most sensitive technique for the detection of $BaCO_3$ by FTIR analysis, $BaCO_3$ concentration down to 0.6% has been estimated [116]. To check the purity and incorporation of Sn^{4+} ion in the lattice of $BaTiO_3$, FTIR spectra of the samples have been recorded and shown in Figure 4.8. The FTIR spectra of these samples were compared with the FTIR spectra of the end members $BaTiO_3$ and $BaSnO_3$. From the literature, it is noted down that in the FTIR spectrum of $BaTiO_3$ and $BaSnO_3$ a sharp peak around 540 cm^{-1} and 640 cm^{-1}, respectively appears which is assigned to TiO_6 and SnO_6 stretching vibration that connected to the barium ion [118,119]. The FTIR spectrum of the

synthesized samples is similar to their end members $BaTiO_3$ and $BaSnO_3$. It is noticed that the position of the strongest peak shifts systematically towards a higher wave number, i.e., towards higher energy with increasing concentration of dopant Sn. This is because the atomic mass of Sn (atomic weight= 118.71 u) is heavier than atomic mass of Ti (atomic mass 47.867u). Therefore, the energy required to set stretching vibration of TiO_6 is less than SnO_6. The shift in the peak position from sample BTS0 to BTS40 is an indication of the incorporation of Sn^{4+} at Ti^{4+} site of $BaTiO_3$.

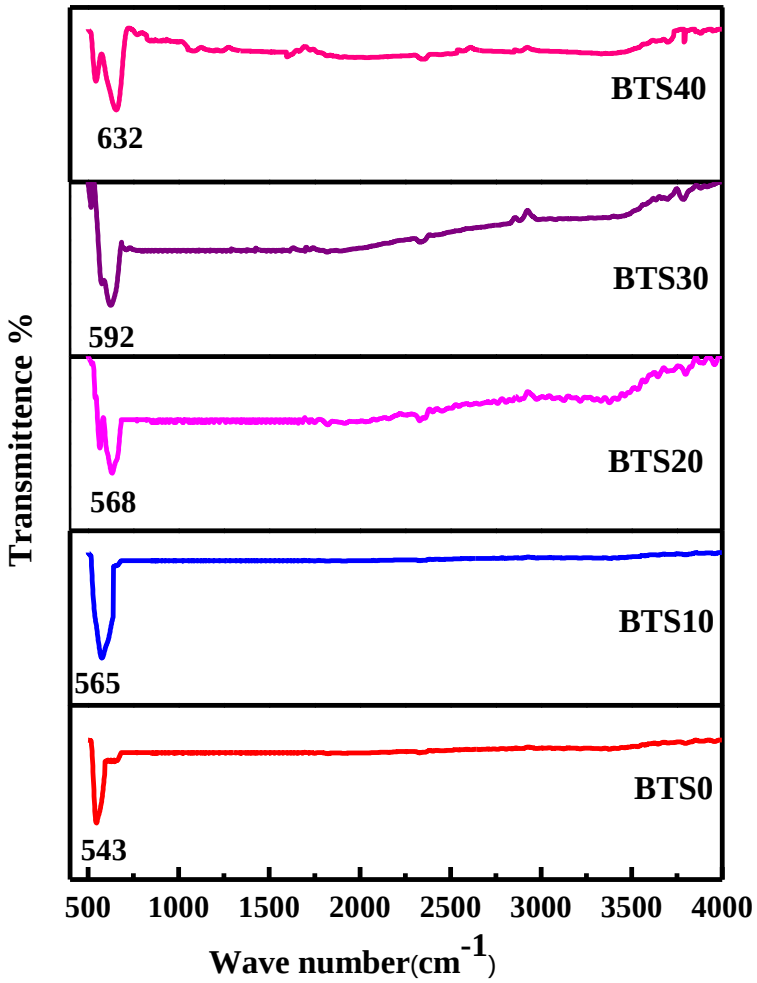

Figure 4.8 Fourier Transform Infra-red spectroscopy (FTIR)of sintered samples

4.4.4 Microstructural Analysis

Scanning electron micrographs (SEM) were obtained to collect information about grain size, shape and the degree of powder agglomeration. The SEM images of the fractured surfaces of ceramics of BTS0, BTS10, BTS20, BTS30 and BTS40 samples are shown in Figure 4.9. The average grain size of samples was determined by the mean of linear intercept method using software 'Image J' and given in Table 4.3**.** As tin contents increase from BTS0 to BTS10, BTS20, BTS30 and BTS40, the average grain size of BTS ceramics slightly decreases from 3.5 μm to 2.5 μm (as shown in Table 4.3). The reduction in grain size with increasing of tin content may be due to lower grain-growth rates on account of larger ionic radii and more massive atomic mass of Sn^{4+} ion than host ion Ti^{4+}. From Table 4.3 it is noticed that grain size of the ceramics prepared in this chapter is many times smaller than the grain size of the same ceramics prepared by conventional solid state using $BaCO_3$ [112]. The small and uniform grain size obtained in this work is attributed to the small particle size (35-50 nm) of calcined powders. The lower calcination temperature (800^oC) is believed to be beneficial to the fine grain size of ceramics.

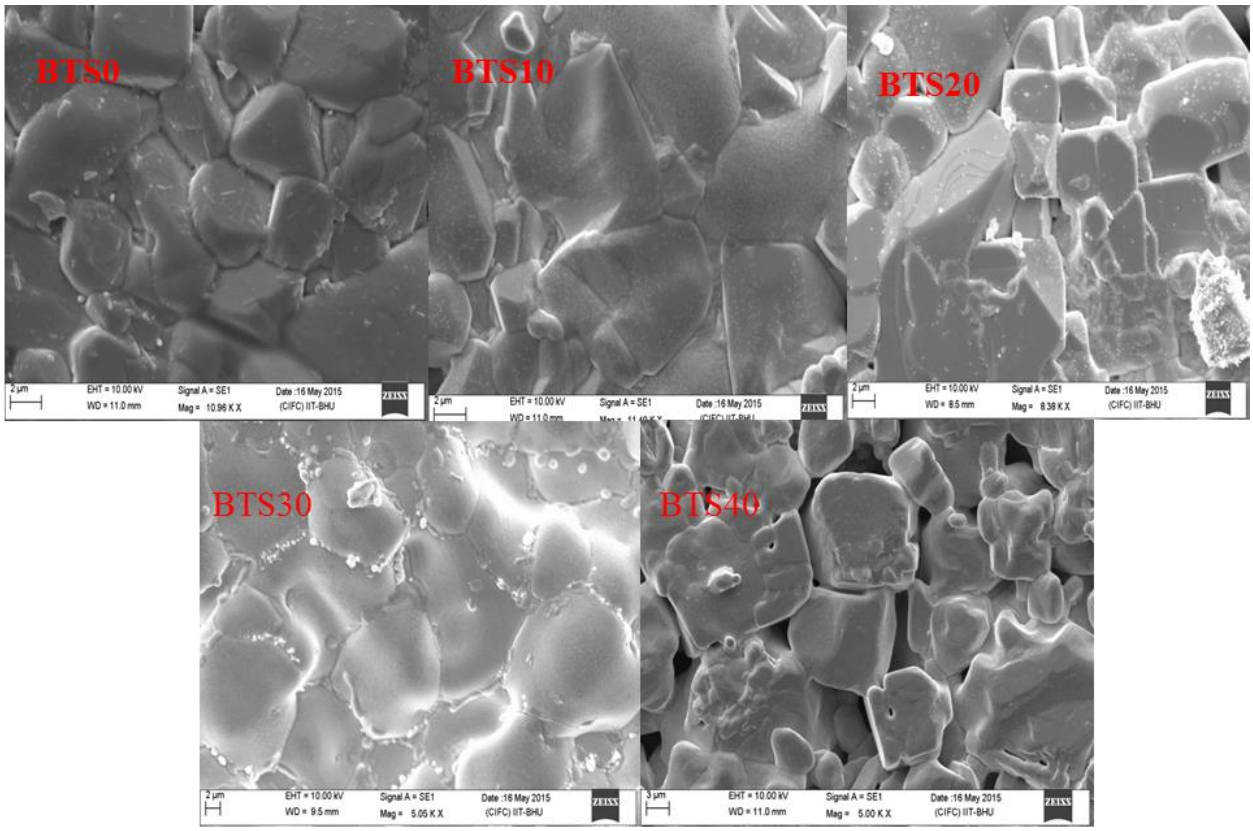

Figure 4.9 Scanning electron micrographs of fractured surface of sintered samples

4.4.5 Energy dispersive x-ray (EDX) Analysis

To check the compositional homogeneity of the synthesized samples, the compositional variation (regarding concentration profile of the elements) has been probed by recording EDXA spectra of different points randomly selected in various grain core and grain boundary regions. Typical EDXA spectra of the samples are shown in Figure 4.10. The positions of all the peaks observed in the Figure. 4.10 are in agreement with EDXA spectra reported for BTS ceramics [110]. It is noted that only peaks of Ba, Ti, Sn and O are present in the EDXA spectra of the samples. All the constituent elements observed in the spectrum of the samples are as per their expected concentrations.

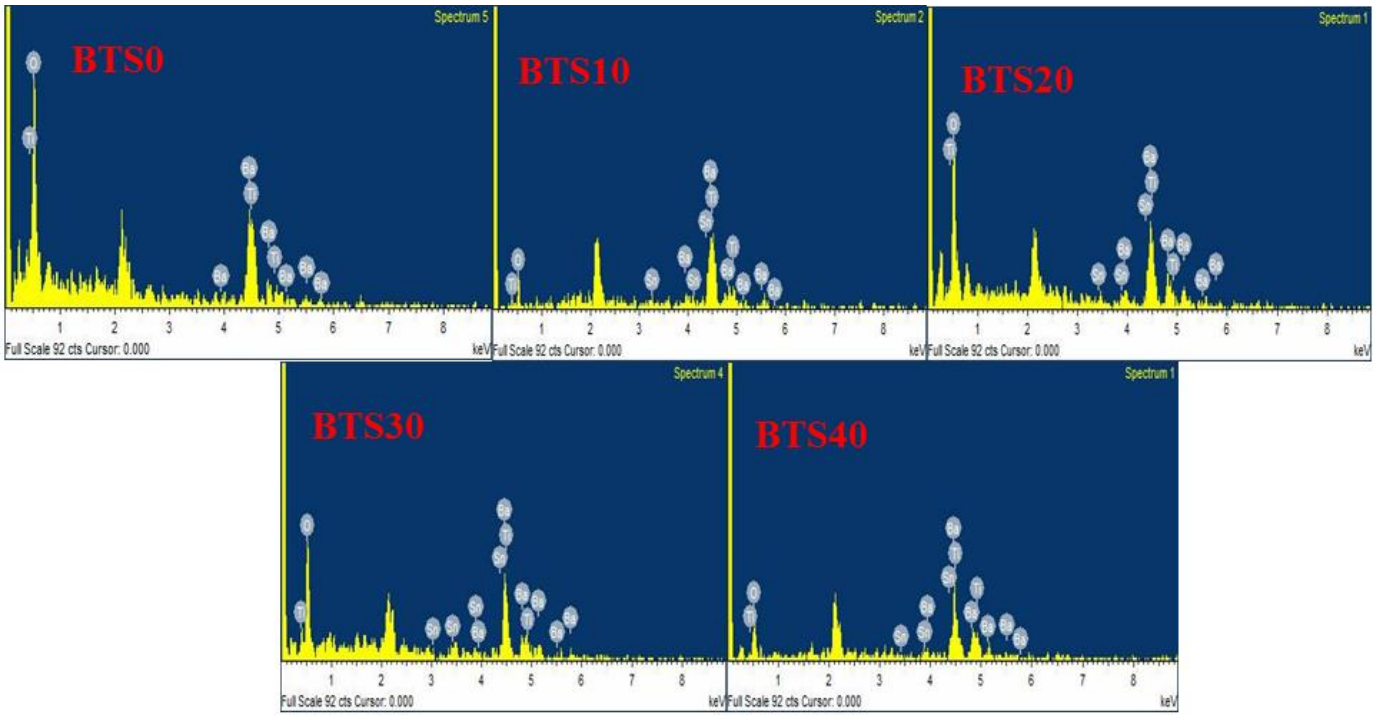

Figure 4.10 Energy dispersive x-ray analysis (EDXA) spectra of sintered samples

4.4.6 Dielectric Analysis

Temperature dependence of dielectric constant (ε) at three different frequencies 1, 10 and 100 kHz for BTS0, BTS10, and BTS20 are shown in Figure 4.11 [(a), (b) and (c)]. We could not be able to measure the dielectric properties of samples BTS30 and BTS40 due to the limitations of the experimental set-up used for the measurement. The plots of ε vs. T for all the three compositions shows that the dielectric constant increases with increasing temperature, reaches a maximum ε_m at a particular temperature T_m, after that it again decreases with increasing temperature indicating a transition at T_m. The plots of ε vs. T as shown in Figure 4.11 reveals that the position of the dielectric peak (ε_m) shifts toward lower temperature side and the value of temperature (T_m) decrease with increasing Sn concentration. This is because in $BaTi_{1-}$

$_xSn_xO_3$ solid solution, Sn^{4+} is distributed uniformly in the unit cells of $BaTiO_3$, which makes the partial unit cells, take on center symmetry at room temperature. The result is that value of T_m (phase transition temperature) at which the structure of BTS ceramics changes from tetragonal to cubic structure shifts progressively towards a lower temperature, that is to say, T_m shifts towards lower temperature side. The decrease in the transition temperature with increasing concentration of Sn in BT is according to the literature [109-112,123]. For the samples BTS0 there is no measurable shift in the value of T_m with frequency and observe a sharp peak, while for the samples BTS10 and BTS20 diffused peak at temperature T_m is observed the value of T_m, ε_m and ε_{RT} at 10 kHz frequency for samples BTS0, BTS10 and BTS20 are tabulated in Table 4.4. To measure diffuseness in the dielectric peak, a modified Curie- Weiss law proposed by Uchino et al. [134] was employed in this chapter. Modified Curie- Weiss law describes the diffuseness of a transition

$$\frac{1}{\in} - \frac{1}{\in m} = \frac{(T - Tm)^{\gamma}}{C} \tag{4.3}$$

Where γ and C are assumed to be constant, ε_m and T_m represent the maximum dielectric constant, and the corresponding temperature has been employed. The parameter γ gives information on the character of the phase transition: γ close to 1 suggests normal ferroelectrics, while close to 2 indicates relaxor ferroelectrics [112]. The plots of log $(1/\varepsilon - 1/\varepsilon_m)$ as a function of log $(T-T_m)$ at 10 kHz for BTS0, BTS10, and BTS20 samples are shown in Figure 4.12. All the samples exhibit a linear relationship. By least-squared fitting the experimental data to the modified Curie-Weiss law, γ was determined. The calculated values γ is given in Table 4.3. The value for BTS0 is 1.12, revealing the characteristic of typical ferroelectric. For BTS10 it is 1.56 and BTS20 it is 2.01, increasing the value of γ with increasing Sn concentration, suggest that with increasing Sn content nature of phase transition become diffuse and relaxor which is

according to the literature. For the comparative study dielectric parameters of same compositions prepared by using different raw materials and methods are given in Table 4.4 [109,111,112, 123].

Figure 4.13 shows the temperature dependences of the dissipation factor of the $BaTi_{1-x}Sn_xO_3$ ceramics with different tin contents at different frequency range 1 kHz, 10 kHz and 100 kHz. Figure 4.13 shows that the dissipation factors for the samples BTS0 almost constant with increasing the temperature at all frequency, but for the sample BTS10, and BTS20 dissipation factor increases with increasing the temperature. For the sample BTS20, the dissipation factor firstly increases after that decreases with increasing temperature.

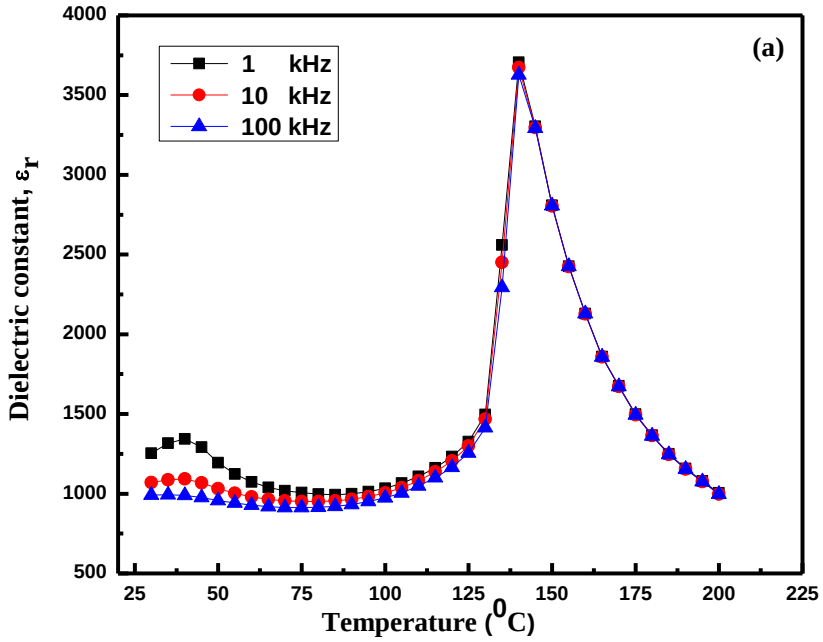

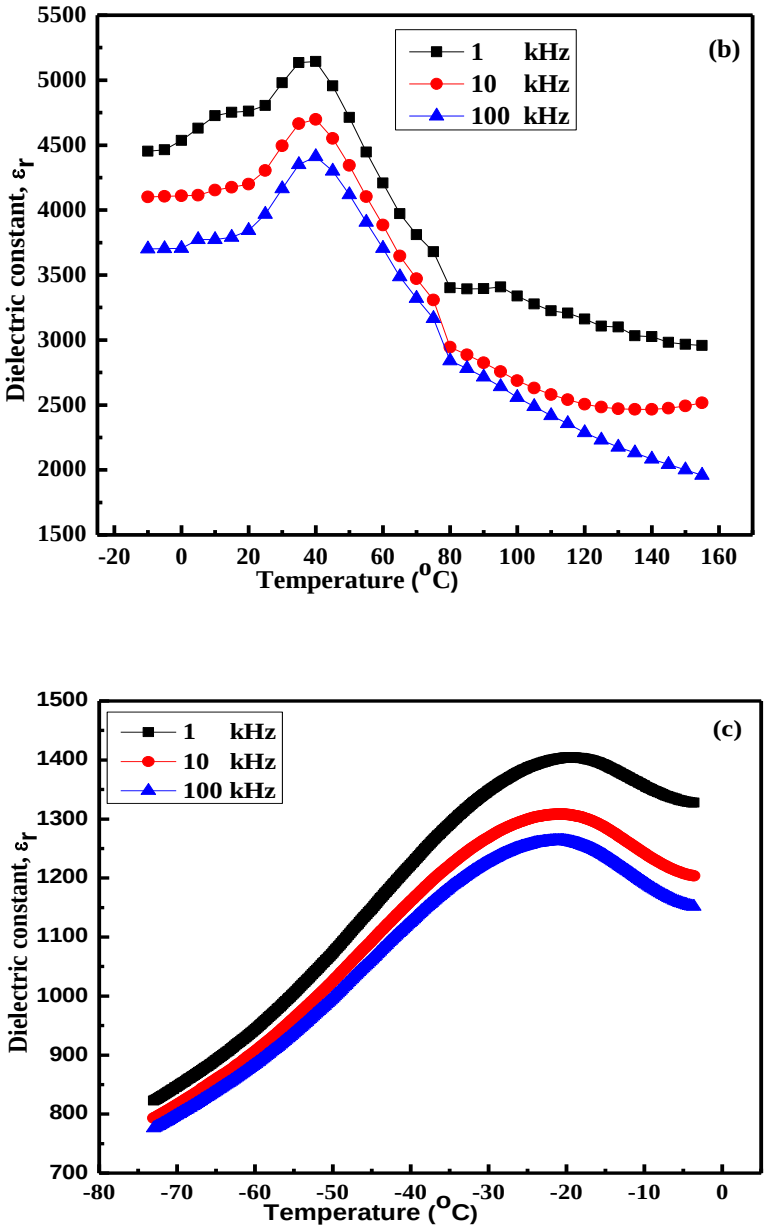

Figure 4.11 Variation of dielectric constant with temperature (a) BTS0 (b) BTS10 and (c) BTS20 at three different frequencies.

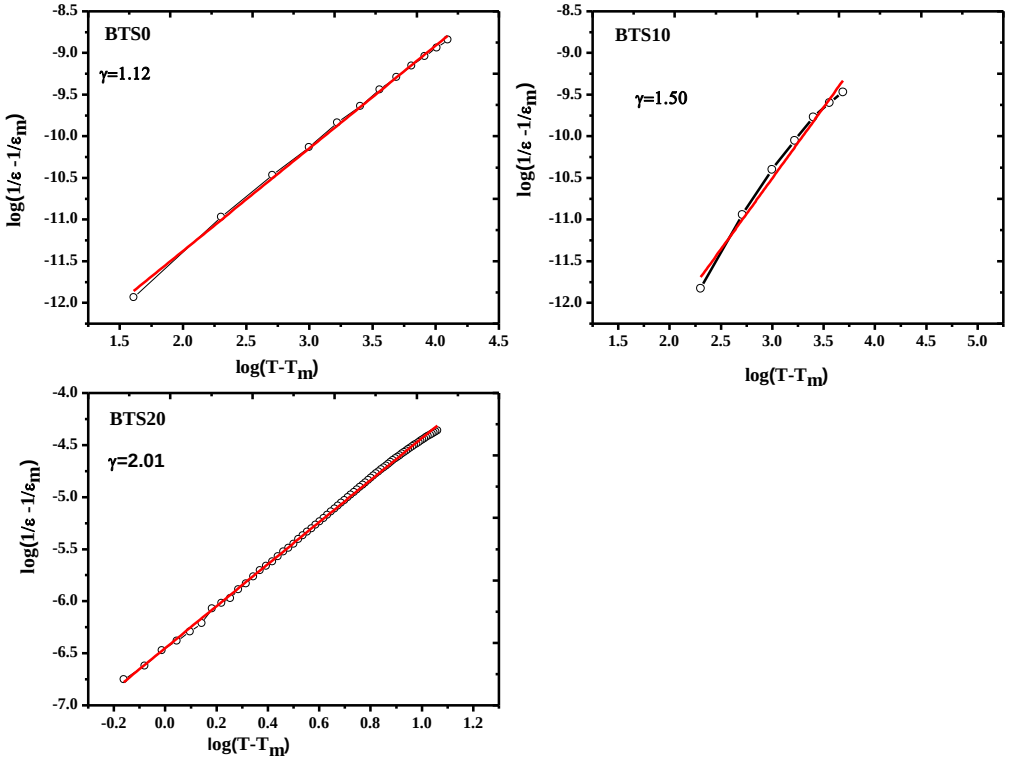

Figure 4.12 Plot of log1/ε - 1/ε_m as a function of log (T - T_m) of Samples at 10kHz

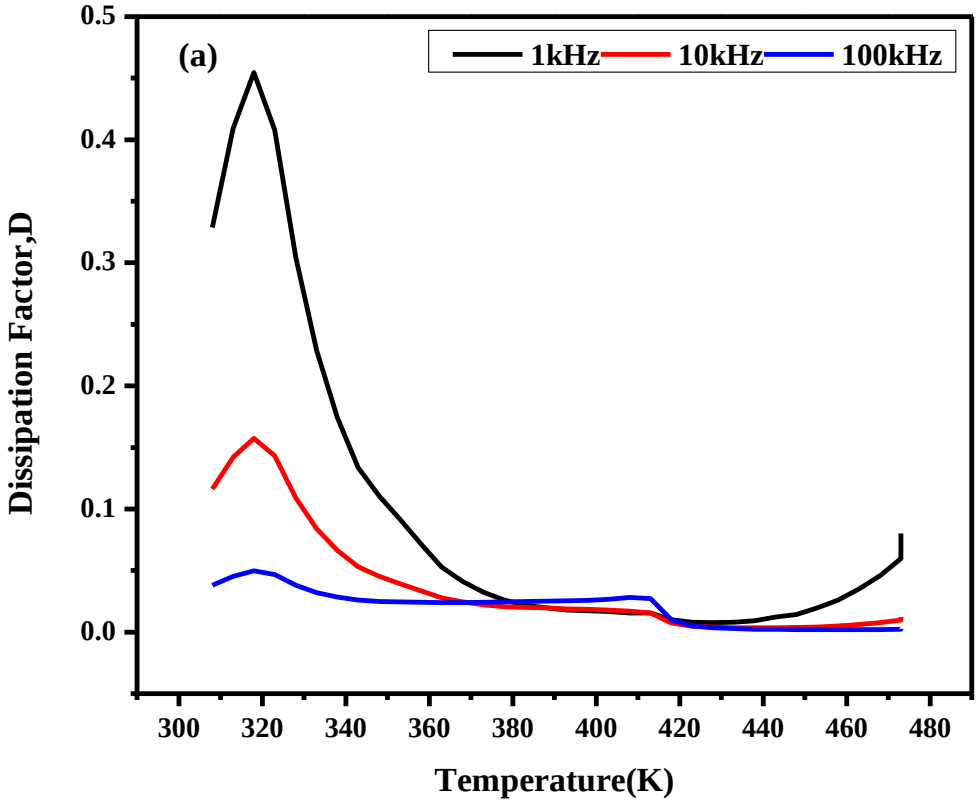
(a)
1kHz
10kHz
100kHz
Dissipation Factor,D
0.5
0.4
0.3
0.2
0.1
0.0
300
320
340
360
380
400
420
440
460
480
Temperature(K)

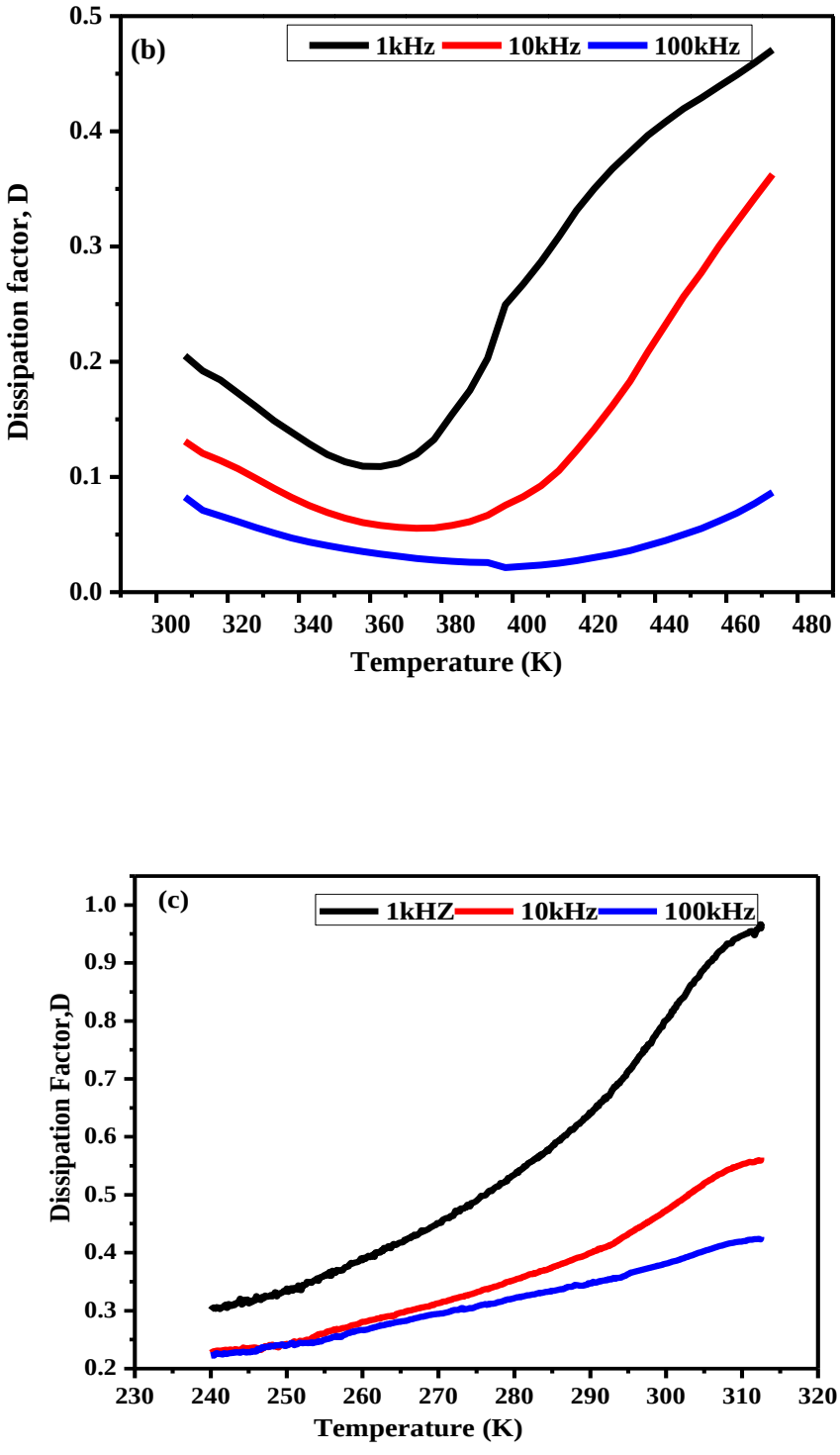

Figure 4.13 Variation of dissipation factor with temperature (a) BTS0 (b) BTS10 (c) BTS20 at three different frequencies

Table 4.4 Comparison (at 10 kHz) of dielectric properties of $BaTi_{1-x}Sn_xO_3$ ceramics

Method	Composition	Grain size (μm)	ϵ_{RT}	ϵ_{max}	T_C	Diffusivity (γ)	P_r ($\mu C/cm^2$)	E_C (kv/cm)	References
Solid State Reaction	0.00 0.10 0.20	44.2 41.3 34.9	----- ----- -----	5363 6695 11219	131 31 -25	1.07 1.29 1.46	Decreases with increasing x	Increases with increasing x	18
Solid State Reaction	0.00 0.10 0.20	80 58 28	1000 1500 2000	6000 12000 8000	120 46.5 -40	1.10 1.42 -----	Decreases with increasing x	Decreases with increasing x	19
Solid State Reaction	0.00 0.10	----- -----	1160 4093	6013 7526	120.8 37.4	----- -----			20
Solid State Reaction	0.00 0.10 0.20	----- 4.6-1.9 -----	----- ----- -----	6916 10029 3445	125 50 -20	1.01 1.65 1.72			21
Sol –gel	0.10 0.20	----- -----	2510 3689	5862 5293	850	----- -----			22
Solid State Reaction	0.0 0.10 0.20 0.30 0.40	3.5 3.2 3.0 2.7 2.5	1221 4123 -----	3824 4610 1296	133 41 -18	1.12 1.50 2.01	5.54 7.65 0.32	9.49 9.63 0.47	This Work

4.4.7 P-E loop

Typical polarization hysteresis loops for BTS0, BTS10, and BTS20 at room temperature and 50 Hz are shown in Figure. 4.14. Strong loop for samples BTS0 and BTS10 confirms ferroelectric nature of these samples at room temperature. Hysteresis loop of BTS0 and BTS10 are not symmetrical about the origin. This asymmetry may be due to internal biasing [135]. The remnant polarization (*P*r) and coercive field (*E*c) values determined from hysteresis loop are given Table 4.5. From the table, it can be seen that P_r for sample BTS10 is larger than BTS0. This may be due smaller grain size of BTS10 than BTS0 because reversal polarization process of a ferroelectric is more complicated inside a small grain than large grain [136].

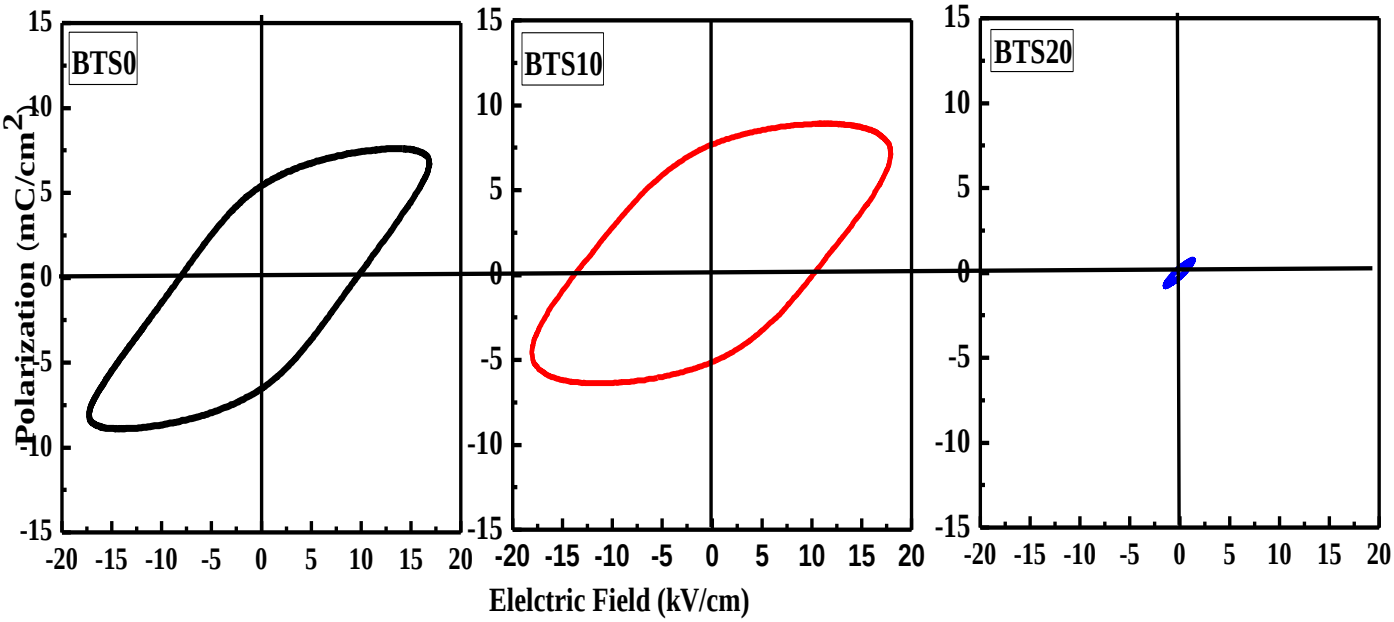

Figure 4.14 Room temperature P-E loop of the ceramic samples

Table 4.5 Dielectric properties of $BaTi1_{-x}Sn_xO_3$ ceramics at 10 kHz

Sample code	Composition	Grain size (μm)	ϵ_{RT}	ϵ_{max}	T_C	Diffusivity (γ)	P_r ($\mu C/cm^2$)	E_C (kv/cm)
BTS0	0.00	3.5	1221	3824	133	1.12	5.54	9.49
BTS10	0.10	3.2	4123	4610	41	1.50	7.65	9.63
BTS20		3.0	-----	1296	-18	2.01	0.32	0.47
BTS30	0.30	2.5	----					
BTS40	0.40	2.7	----					

4.5 CONCLUSIONS

Single phase powders nano-sized powders of solid solutions, $BaTi_{1-x}Sn_xO_3$ (x=0.0, 0.1, 0.2 0.3 and 0.40) were successfully synthesized by the solid state route using $Ba(NO_3)_2$, TiO_2 and $SnCl_45H_2O$ followed by calcination at 800 ^oC for 8 h. X-ray diffraction technique has confirmed that synthesized powders of composition x=0.0 and 0.10 have tetragonal whereas x=0.20 and 0.30 have a cubic crystal structure. Transmission electron microscopic studies confirmed that particles of calcined powders have a spherical shape with diameter 30-50 nm. The microstructure of BTS ceramics synthesized in this work has small and uniform grain size as compared to same ceramics synthesized by conventional solid state route using oxide or carbonate as starting materials. Thermal analysis (simultaneous TGA/DSC) of the raw materials as well as of a mixture of these raw materials has confirmed that the formation of reliable solid solutions in this method takes place between 600-700^oC. The formation of BTS system proceeds while heating up in three steps : (i) formation of SnO_2 from $SnCl_4$ $5H_2O$, (ii) melting of $Ba(NO_3)_2$ and (iii) reaction among molten $Ba(NO_3)_2$ and TiO_2 and SnO_2 (solid form). Therefore,

we can conclude that replacement of $BaCO_3$ by $Ba(NO_2)_3$ as raw materials for the mass production of nanopowders of BTS for industrial applications is a cost-efficient and straightforward method as compared to other methods reported in the literature.